SLAC-PUB-1857
LBL-5590
December 1976
(T/E)

# INCLUSIVE $\rho^0$ PRODUCTION IN $\gamma p$ INTERACTIONS AT 2.8, 4.7, AND 9.3 GeV*

E. Kogan, J. Ballam, G. B. Chadwick, K. C. Moffeit, P. Seyboth†, I. O. Skillicorn‡, H. Spitzer§, and G. Wolf††

Stanford Linear Accelerator Center
Stanford University, Stanford, California 94305

H. H. Bingham, W. B. Fretter, W. J. Podolsky‡‡, M. S. Rabin§§, A. H. Rosenfeld, and G. Smadja†††

University of California and Lawrence Berkeley Laboratory
Berkeley, California 94720

Y. Eisenberg

Department of Nuclear Physics, Weizmann Institute of Science
Rehovot, Israel

(Submitted to Nucl. Phys. B)

*Work supported by the Energy Research and Development Administration and the National Science Foundation.

Present address:
†Max-Planck-Institut für Physik und Astrophysik, München, Germany
‡University of Glasgow, Glasgow, Scotland
§University of Hamburg, Hamburg, Germany
††DESY, Hamburg, Germany
‡‡Stanford University Medical Center, Stanford, California
§§University of Massachusetts, Amherst, Massachusetts
†††DPHPE, CEN, Saclay, France

ABSTRACT

Inclusive $\rho^o$ production in $\gamma p \to \rho^o$ + anything is studied at 2.8, 4.7, and 9.3 GeV, using the SLAC linearly polarized backscattered laser photon beam and the 82" hydrogen bubble chamber. Over this energy range the inclusive inelastic $\rho^o$ cross section rises from 6.0 $\mu$b to 20.5 $\mu$b. The multiplicity, i.e., the average number of $\rho^o$ mesons per inelastic hadronic event, has an energy dependence consistent with ln s.

The inclusive cross section is studied as a function of Feynman x, c.m. rapidity, and $p_T^2$ variables, and is also broken down into exclusive channels. At 9.3 GeV a forward inelastic peak is observed in the x distribution, containing mainly polarized $\rho^o$ mesons. The cross section for this inelastic diffractive component is 2.7 ± 0.6 $\mu$b. The $p_T^2$ distributions are exponential with a slope of 3 - 4 $(\mathrm{GeV}/c)^{-2}$, similar to that found in inclusive $\rho^o$ production in pp and $\pi$p reactions.

## 1. Introduction

Quasi-elastic $\rho^o$ photoproduction in the exclusive reaction $\gamma p \rightarrow p\rho^o$ plays the role of elastic scattering in hadronic interactions. Its study has been a powerful probe of the hadronic component of the photon. In contrast little information is available on inelastic $\rho^o$ photoproduction.

Recently it has been shown [1-3] that inclusive $\rho^o$ production in pp and $\pi p$ reactions is quite substantial and grows logarithmically with energy. It accounts for a considerable fraction of charged pion production and of lepton pairs. The question arises whether inclusive $\rho^o$ production plays a similar role in $\gamma p$ reactions [4]. The study of inclusive $\rho^o$ photoproduction has the added interest that leading particle effects ($\gamma \rightarrow \rho^o$) can be studied. In particular, with a polarized photon beam one can determine the cross section for diffraction dissociation $\gamma p \rightarrow \rho^o X$ (X = nucleon + $\pi$'s) via an s-channel helicity conserving (SCHC) natural-parity exchange mechanism.

In this paper we present a measurement of inclusive inelastic $\rho^o$ production by linearly polarized photons at energies $E_\gamma = 2.8$, 4.7, and 9.3 GeV. The data were obtained from exposures of the 82" bubble chamber to the backscattered laser beam at SLAC. Our experimental setup and film analysis procedures have been reported in refs. [5,6]. The use of a bubble chamber allows an easy separation of quasi-elastic $\rho^o$ production via $\gamma p \rightarrow p\rho^o$ from inelastic $\rho^o$ production via $\gamma p \rightarrow \rho^o X$. This is important because we wish to compare our results for the latter reaction with those from inclusive studies of $\pi p$ or pp reactions, where the elastic scattering events are excluded. Our results on quasi-elastic $\rho^o$ production have already been reported [5], as has our analysis of inclusive $\pi^-$ production [7].

## 2. Determination of Inclusive $\rho^o$ Cross Sections

We include in our analysis all measured events without a visible strange particle decay, except those fitting the reactions $\gamma p \rightarrow p\pi^+\pi^-$, $pK^+K^-$ and $pp\bar{p}$ [5]. For particle momenta $<1.5$ GeV/c it was possible to distinguish pions from protons by ionization (below 0.8 GeV/c K-$\pi$ separation was also possible). In cases of ambiguity, charged tracks were taken to be pions.

Figures 1-3 show the inclusive invariant mass distributions for all $\pi^+\pi^-$ combinations at the three energies. We also show the mass distributions for four intervals of the $\pi^+\pi^-$ pair Feynman x variable ($x = p_L^*/p_{max}^*$ - the asterisk denotes the c.m. system).

To determine cross sections and invariant structure functions $F(x) = \frac{1}{\pi}\frac{E^*}{p_{max}^*}\frac{d\sigma}{dx}$, we divided the data into x-intervals and fitted the mass distributions to a relativistic p-wave Breit-Wigner† with a mass skewing factor $(M_\rho/M_{\pi\pi})^n$ for the $\rho^o$, plus a second-order polynomial†† in $M_{\pi^+\pi^-}$ for the background. The mass skewing is discussed below. The fits were done in the mass range $0.52 < M_{\pi^+\pi^-} < 1.16$ GeV, weighting each event by its detection efficiency [6]. For the $\rho^o$ we assumed a fixed mass of 0.765 GeV and a fixed width of 0.145 GeV. The resulting fits are indicated by full lines in figs. 1-3, while the background is indicated by dashed lines. Our procedure is the same as that used by refs. [1,2a,3b,3d] in hadron-initiated reactions.

Table I gives the resulting cross sections at the three energies for four x intervals, and the total inelastic $\rho^o$ cross section obtained by fitting the

†As in Appendix A of ref. [5].

††Generally a second-order polynomial led to statistically acceptable fits and described well the $\pi^+\pi^+$ and $\pi^-\pi^-$ mass distributions. Fitting with a third-order polynomial yielded usually results within one standard deviation, with the coefficient of the third power consistent with zero. When occasionally the fit improved by adding a third-order term, that fit was used.

inclusive mass distribution for all x. The $\chi^2$ per degree of freedom for each fit is given in the last column of table I. The errors are statistical only; varying the $\rho^0$ width by ± 10 MeV changes the quoted cross sections by 3-9%, which is within one standard deviation.

Previous studies of quasi-elastic $\rho^0$ photoproduction have shown that the $\rho^0$ interferes with a p-wave $\pi^+\pi^-$ background [5]. This interference induces changes in the mass shape which can be well described phenomenologically by a mass skewing factor $(M_\rho/M_{\pi\pi})^n$ [5]. We have included such a factor in our fits and investigated the dependence of n on x. The values found for n(x) in the four x intervals are also listed in table I. At 9.3 GeV, n(x) increases as x approaches its upper limit, and in the forward direction is similar to the value found in quasi-elastic $\rho^0$ photoproduction [5]. At 4.7 and 2.8 GeV, no appreciable skewing nor systematic dependence of n on x were found, and average fixed values of +1 and 0 respectively were used throughout. All cross sections have been corrected by 5-7% to account for the $\rho^0$ tails outside the fitted mass range.

## 3. Results and Discussion

In fig. 4 we show $d\sigma/dy_{c.m.}$ for inelastic $\rho^0$ production at the three energies obtained by similar fits. The $\rho^0$ is produced predominantly in the forward hemisphere (63, 68, and 71% at 2.8, 4.7, and 9.3 GeV, respectively).

The invariant structure function F(x) for inelastic $\rho^0$ production is shown in fig. 5 for the 2.8 and 4.7 GeV data and in fig. 6 for the 9.3 GeV data. The curve in fig. 6 describes the $\gamma p \to \pi^- X$ data from ref. [7] normalized by the ratio of the $\rho^{o}$ to $\pi^{-}$ multiplicities at this energy. The data in figs. 5-6 are presented in smaller x bins than those given in table I, in order to emphasize the structure of the cross section. Fig. 6 indicates that the 9.3 GeV cross section is composed of two components: (a) a broad distribution similar to F(x) for inclusive $\pi^{-}$ photoproduction which peaks near x = 0, and (b) a photon diffraction dissociation forward peak which rises rapidly from x = 0.75 to the forward kinematical limit.

In fig. 7 we show evidence that the leading $\rho^{o}$'s in the diffraction forward peak are polarized like the photon beam. We plot the distributions of cos $\theta_H$ and $\psi_H$, where $\theta_H$ is the polar angle of the decay $\pi^{+}$ in the s-channel helicity system, and $\psi_H$ is its azimuth with respect to the beam polarization plane (as defined in ref. [5]). We plot the angles for all $\pi^{+}\pi^{-}$ pairs in the $\rho$ mass region and forward x interval. In the helicity frame we observe the characteristic $\sin^2\theta_H$ and $\cos^2\psi_H$ signals of an s-channel helicity conserving (SCHC) $\rho^{o}$ above the background. This feature is similar to quasi-elastic $\rho^{o}$ photoproduction [5]. It was observed first in the inelastic inclusive $\pi^{-}$ azimuthal distribution at 9.3 GeV in ref. [7]. In the Gottfried-Jackson and Adair frames [5], the cos $\theta$ distribution (also shown in the figure) is more isotropic, indicating the production mechanism is better described by SCHC than by t-channel helicity conserving or spin-independent models [5].

In ref. [5] we defined a cross section for SCHC and natural-parity exchange $\rho^{o}$ production as

$$\Pi = \frac{1}{P_\gamma}\left(\frac{40\pi}{3}\right)^{\frac{1}{2}}\sum \mathrm{Re}\,Y_2^2(\theta_H,\psi_H) = \frac{2.5}{P_\gamma}\sum \sin^2\theta_H \cos 2\psi_H$$

where $P_\gamma$ stands for the degree of linear polarization of the photon beam [5]. $\Pi$ is shown in fig. 8 as a function of $M_{\pi^+\pi^-}$ for the two forward x-intervals at

$E_\gamma = 4.7$, 9.3 GeV. No SCHC $\rho^0$ signal is observed in the other two intervals or at 2.8 GeV. The resulting cross sections $\sigma_{DIFF}$, obtained by summing over the mass distributions in fig. 8, are given in table I and plotted as a function of x in fig. 6. Quantitatively we find that 60% of the 9.3 GeV cross section for $x > 0.8$ is due to SCHC $\rho^0$ events. Using the SCHC cross section at 9.3 GeV as an estimate of inelastic diffractive $\rho^0$ production, we obtain $2.7 \pm 0.6\ \mu b$, in agreement with a theoretical estimate by G. Wolf [8]. Thus we conclude that, like elastic hadron scattering and quasi-elastic $\rho^0$ photoproduction [5], the diffraction dissociation of the photon into a rho seems to be a dominantly s-channel helicity conserving process. This supports the view that approximate SCHC is a universal property of Pomeron exchange, in both elastic and inelastic processes [9].

In fig. 9 we compare F(x) at 9.3 GeV (normalized to $\sigma_{inel.}(\gamma p)$) to a typical leading particle distribution in hadronic collisions, namely, $\pi^+ p \rightarrow \pi^+ X$ at 7 GeV/c [10] (normalized to $\sigma_{inel.}(\pi p)$). The two are roughly similar in shape. We also plot the result for $\pi^+ p \rightarrow \rho^0 X$ at 16 GeV/c [2b]. It agrees with the photoproduction data in magnitude and shape, except for the forward diffractive peak in the photoproduction data.

In table II we relate our inclusive results to $\rho^0$ cross sections in the exclusive channels.* We note that most of the diffractive SCHC cross section is due to 3- and 4-body events (counting the $\rho^0$ as one body), resembling the behavior of the diffractive component in hadronic reactions at very high energies [11]. We also note that a part of the 9.3 GeV SCHC $\rho^0$ signal in the $p2\pi^+2\pi^-$ channel is

*The sums of the exclusive $\rho^0$ cross sections in table II agree within errors with the total $\rho^0$ cross sections from table I and hence confirm the internal consistency of the fitting procedure.

due to polarized $\rho''(1600)$ production [12]. At 4.7 GeV the SCHC signal comes entirely from the $n2\pi^+\pi^-$ channel.

The inclusive inelastic $\rho^0$ cross sections at the three energies are summarized in table III. For completeness the quasi-elastic $\gamma p \rightarrow p\rho^0$ cross sections [5], as computed by more elaborate maximum likelihood fits, are also given. Using the same mass fits as for the inelastic events, we obtain cross sections which agree within 6%. The resulting multiplicities for both total and inelastic $\rho^0$ production are also listed in the table.

Comparing the $\pi^-$ average multiplicities in this experiment [7], with the total $\rho^0$ multiplicities at the three energies, we observe that the $\rho^0/\pi^-$ ratio is roughly constant at 22-25%. This would give a contribution to direct lepton photoproduction of $e^-/\pi^- \sim 10^{-5}$.

We note the interesting fact that, although the quasi-elastic cross section decreases with energy, the increasing inclusive inelastic cross section more than compensates for this decrease, and thus the total inclusive $\rho^0$ cross section and multiplicity are rising. In fact, both the total and inelastic multiplicities can be well described by a logarithmic rise, and a fit yields:

$$<\rho^0>^I = (-0.18 \pm 0.04) + (0.13 \pm 0.02) \ln s$$

$$<\rho^0>^T = (\ 0.09 \pm 0.05) + (0.07 \pm 0.02) \ln s$$

where I and T denote the inelastic and total multiplicities, respectively. If the coefficient of ln s in the first equation is an indication of the high energy behavior, the height of the (asymptotic) plateau in the rapidity distribution should be about 13 $\mu$b, and this seems to be reached already at 9.3 GeV.

At $E_\gamma = 9.3$ GeV the $\rho^0/\pi^-$ ratio (with the quasi-elastic $\rho^0$ contribution taken out in both numerator and denominator) is $0.16 \pm 0.02$. This is to be compared with a constant $\rho^0/\pi^-$ ratio of $0.19 \pm 0.02$ in $\pi^+p \rightarrow \rho^0X$ at 8, 16, and 23 GeV/c [2b], and $0.20 \pm 0.02$ in $\pi^-p \rightarrow \rho^0X$ at 16 GeV/c (where the leading $\pi^-$ is excluded [3e]). In all three processes the $\rho^0$ is produced both by central resonance production and by beam fragmentation [2b, 3e].

Finally we present in fig. 10 $d\sigma/dp_T^2$ at the three energies. These cross sections are fitted to a simple exponential of the form $Ae^{Bp_T^2}$, for $p_T^2 < 0.8$ $(GeV/c)^2$. The resulting slopes B are given in table IV. They are typically 3-4 $(GeV/c)^{-2}$ and similar to the slopes found for $\rho^0$ inclusive production in hadronic collisions [2b, 3e], as compared to a slope of around 6 $(GeV/c)^{-2}$ for pion photoproduction [7] and nonleading pion production in $\pi p$ collisions [2b, 3e]. Thus the $\rho^0/\pi^-$ ratio increases with $p_T^2$ in the low $p_T^2$ region accessible to this experiment.

Table IV also shows the average $<p_T^2>$ for the four x-intervals. In the forward x-region $<p_T^2>$ is smaller than the average (i.e., the slope is higher). This is a kinematical effect due to phase space limitations. However, the surprising feature is that $<p_T^2>$ continues to increase as x approaches 0, as opposed to the dip at $x = 0$ (sea gull effect [13]) seen for pions [7]. This again is in agreement with the behavior observed for $\rho^0$ production in hadronic processes [2a, 3].

In conclusion we observe that at energies of 3-10 GeV the total $\rho^0$ inclusive cross section is substantial, and the $\rho^0$ multiplicity is consistent with a logarithmic increase with s. The inelastic $\rho^0$'s are predominantly emitted in the forward hemisphere, with an exponential $p_T^2$ distribution which is flatter than that for pions. At 9.3 GeV we observe for $0.8 < x < 1.0$ a $2.7 \pm 0.6$ $\mu b$ signal of helicity conserving polarized inelastic $\rho^0$'s, recoiling against a low mass baryon-pion system, the analog of inelastic diffraction in hadronic reactions.

## Acknowledgements

We wish to thank the SLAC Operations Crew, R. Watt, and the 82" Bubble Chamber Operations Group for their assistance in performing this experiment. We thank R. Gearhart, J. J. Murray, and C. K. Sinclair for their help during the early stages of the experiment. We acknowledge the diligence of our scanners and our data reduction group, in particular D. Blohm, K. Eyman, W. Hendricks, and A. Wang.

References

[1] For $pp \to \rho^0 X$ see:

(a) V. Blobel et al., Phys. Lett. 48B (1974) 73;

(b) R. Singer et al., Phys. Lett. 60B (1976) 385.

[2] For $\pi^+ p \to \rho^0 X$ see:

(a) H. A. Gordon et al., Phys. Rev. Lett. 34 (1975) 284;

(b) M. Deutschmann et al., Nucl. Phys. B 103 (1976) 426.

[3] For $\pi^- p \to \rho^0 X$ see:

(a) P. Borzatta et al., Nuovo Cimento 15A (1973) 45;

(b) J. Brau et al., Nucl. Phys. B 99 (1975) 232;

(c) D. Fong et al., Phys. Lett. 60B (1975) 124;

(d) F. C. Winkelmann et al., Phys. Lett. 56B (1975) 101;

(e) J. Bartke et al., Nucl. Phys. B 107 (1976) 93.

[4] For $\gamma N \to \rho^0 X$ see: J. Gandsman et al., Nucl. Phys. B 61 (1973) 32.

[5] J. Ballam et al., Phys. Rev. D 5 (1972) 545; ibid., D 7 (1973) 3150.

[6] H. H. Bingham et al., Phys. Rev. D 8 (1973) 1277.

[7] K. C. Moffeit et al., Phys. Rev. D 5 (1972) 1603.

[8] G. Wolf, Nucl. Phys. B 26 (1971) 317.

[9] G. Chadwick, Y. Eisenberg, and E. Kogan, Phys. Rev. D 8 (1973) 1607.

[10] M. Alston-Garnjost et al., Phys. Lett. 39B (1972) 402.

[11] F. C. Winkelmann et al., Phys. Rev. Lett. 32 (1974) 121; J. W. Chapman et al., Phys. Rev. Lett. 32 (1974) 257.

[12] H. H. Bingham et al., Phys. Lett. 41B (1972) 635.

[13] D. R. O. Morrison, in Proc. 5th Hawaii Topical Conf. in Particle Physics, ed. P. N. Dobson, V. Z. Peterson, and S. F. Tuan (University of Hawaii Press, Honolulu, 1974), p. 189.

TABLE I

Reaction $\gamma p \rightarrow \pi^+\pi^- X$ ($X$ = nucleon + $m\pi$'s, $m \geq 1$). Inclusive $\rho^0$ cross sections, mass skewing parameter n and $\chi^2$ per degree of freedom, as obtained from fits to the $\pi^+\pi^-$ mass distributions for various intervals of Feynman x. $\sigma_{DIFF}$ is the cross section for $\rho^0$ production via SCHC and natural-parity exchange.

| $E_\gamma$ (GeV) | x Interval | $\sigma(\rho^0)$ ($\mu$b) | $\sigma_{DIFF}(\rho^0)$ ($\mu$b) | n(x) | $\chi^2$/D.F. |
|---|---|---|---|---|---|
| 2.8 | (-1.0) - (-0.3) | 0.8±0.4 | * | 0.0 | 18/12 |
| | (-0.3) - ( 0.3) | 2.8±0.9 | * | 0.0 | 11/12 |
| | (0.3) - (0.8) | 2.2±0.7 | * | 0.0 | 12/12 |
| | (0.8) - (0.92) | 0.19±0.17 | * | 0.0 | 10/12 |
| | Sum | 6.0±1.2 | * | | |
| | Inclusive fit | 6.1±1.2 | | 0.0 | 10/12 |
| 4.7 | (-1.0) - (-0.3) | 1.8±0.4 | * | 1.0 | 6/12 |
| | (-0.3) - ( 0.3) | 4.9±0.9 | * | 1.0 | 17/12 |
| | (0.3) - (0.8) | 5.3±0.7 | 0.6±0.4 | 1.0 | 28/12 |
| | (0.8) - (0.96) | 1.1±0.2 | 0.3±0.1 | 1.0 | 19/12 |
| | Sum | 13.1±1.2 | 0.9±0.4 | | |
| | Inclusive fit | 13.9±1.3 | | 1.0 | 37/12 |
| 9.3 | (-1.0) - (-0.3) | 1.6±0.3 | * | 0.6±0.1 | 9/11 |
| | (-0.3) - ( 0.3) | 8.5±0.9 | * | 2.2±1.1 | 21/10 |
| | (0.3) - (0.8) | 7.9±0.6 | 1.2±0.5 | 2.0±0.1 | 14/11 |
| | (0.8) - (1.0) | 2.5±0.2 | 1.5±0.2 | 4.1±0.6 | 6/11 |
| | Sum | 20.5±1.1 | 2.7±0.6 | | |
| | Inclusive fit | 19.9±1.2 | 2.7±1.0 | 1.7±0.8 | 27/11 |

*These values are consistent with zero within one standard deviation and do not show any trend in the $\rho$ mass region, and thus were not included in the sums.

TABLE II

Total and diffractive (SCHC) $\rho^o$ cross sections in the various exclusive channels at $E_\gamma = 2.8$, 4.7, and 9.3 GeV.

| Channel | 9.3 GeV | | 4.7 GeV | | 2.8 GeV |
|---|---|---|---|---|---|
| | $\sigma(\rho^o)$ ($\mu$b) | $\sigma_{DIFF}(\rho^o)$ ($\mu$b) | $\sigma(\rho^o)$ ($\mu$b) | $\sigma_{DIFF}(\rho^o)$ ($\mu$b) | $\sigma(\rho^o)$ ($\mu$b) |
| $p\pi^+\pi^-\pi^o$ | 0.8±0.2 | 0.5±0.2 | 1.2±0.4 | * | 1.8±0.6 |
| $n\ 2\pi^+\pi^-$ | 1.9±0.2 | 0.7±0.2 | 4.1±0.5 | 1.0±0.4 | 3.8±0.7 |
| Multineutral | 4.0±0.5 | 0.8±0.4 | 2.8±0.7 | * | 0.0±0.5 |
| Sum 3 prongs | 6.6±0.6 | 2.0±0.5 | 8.1±0.9 | 1.0±0.4 | 5.6±1.1 |
| $p\ 2\pi^+2\pi^-$ | 3.5±0.3 | 1.2±0.3 | 3.4±0.5 | * | 1.5±0.5 |
| $p\ 2\pi^+2\pi^-\pi^o$ | 1.2±0.3 | * | 1.1±0.4 | * | - |
| $n\ 3\pi^+2\pi^-$ | 2.1±0.4 | * | 1.6±0.4 | * | - |
| Multineutral | 4.3±0.7 | * | - | - | - |
| $pK^+K^-\pi^+\pi^-$ | 0.1±0.06 | * | 0.1±0.07 | * | - |
| Sum 5 prongs | 11.2±0.9 | 1.2±0.3 | 6.2±0.8 | * | 1.5±0.5 |
| $p\ 3\pi^+3\pi^-$ | 1.2±0.2 | * | 0.2±0.1 | * | - |
| $p\ 3\pi^+3\pi^-\pi^o$ | 1.0±0.2 | * | - | - | - |
| $n\ 4\pi^+3\pi^-$ | 1.1±0.3 | * | - | - | - |
| $pK^+K^-2\pi^+2\pi^-$ | 0.08±0.04 | * | - | - | - |
| Sum 7 prongs | 3.4±0.6 | * | 0.2±0.1 | * | - |
| Sum | 21.2±1.3 | 3.2±0.6 | 14.5 1.2 | 1.0±0.4 | 7.1±1.2 |

*These values are consistent with zero within one standard deviation and do not show any trend in the $\rho^o$ mass region, and thus were not included in the sums.

TABLE III

Inclusive $\rho^o$ cross sections and multiplicities.

| $E_\gamma$ (GeV) | s ($GeV^2$) | $\sigma(\rho^o)$ ($\mu b$) | | | $\sigma_{inel.}(\gamma p)$* ($\mu b$) (Refs. 5,6) | $\langle\rho^o\rangle$ | |
|---|---|---|---|---|---|---|---|
| | | Inclusive Inelastic | Quasi-elastic (Ref.5) | Inclusive Total | | Inelastic | Total† |
| 2.8 | 6.1 | 6.0±1.2 | 21.0±1.0 | 27.0±1.6 | 102.9±3.2 | 0.06±0.01 | 0.22±0.01 |
| 4.7 | 9.7 | 13.1±1.2 | 16.2±0.7 | 29.3±1.4 | 102.1±3.1 | 0.13±0.01 | 0.25±0.01 |
| 9.3 | 18.3 | 20.5±1.1 | 13.3±0.5 | 33.8±1.2 | 100.9±2.6 | 0.21±0.01 | 0.30±0.01 |

*Total $\gamma p$ cross section excluding the quasi-elastic reaction $\gamma p \rightarrow p\rho^o$ and events with visible strange particle decays.

†Including quasi-elastic $\rho^o$ production.

TABLE IV

Average transverse momentum squared in four intervals of Feynman x and the slope B of the $p_T^2$ distribution at $E_\gamma$ = 2.8, 4.7, and 9.3 GeV.

| $E_\gamma$ (GeV) | $\langle p_T^2 \rangle$ $(GeV/c)^2$ | | | | | B $(GeV/c)^{-2}$ |
|---|---|---|---|---|---|---|
| | -1<x<-0.3 | -0.3<x<0.3 | 0.3<x<0.8 | 0.8<x<1 | All x | |
| 2.8 | 0.23±0.08 | 0.30±0.07 | 0.20±0.07 | 0.13±0.13 | 0.25±0.04 | 3.7±0.7 |
| 4.7 | 0.26±0.05 | 0.33±0.06 | 0.28±0.04 | 0.09±0.02 | 0.28±0.03 | 3.1±0.4 |
| 9.3 | 0.37±0.08 | 0.35±0.05 | 0.30±0.03 | 0.18±0.03 | 0.31±0.02 | 3.6±0.3 |

Figure Captions

1. Effective mass distributions of the $\pi^+\pi^-$ pairs at $E_\gamma = 9.3$ GeV, for various intervals of the Feynman x variable, as well as the overall mass distribution. Curves are results of fits to $\rho^0$ and background (see text).

2. Effective mass distributions of the $\pi^+\pi^-$ pairs at $E_\gamma = 4.7$ GeV, for various intervals of the Feynman x variable, as well as the overall mass distribution. Curves are results of fits to $\rho^0$ and background (see text).

3. Effective mass distributions of the $\pi^+\pi^-$ pairs at $E_\gamma = 2.8$ GeV, for various intervals of the Feynman x variable, as well as the overall mass distribution. Curves are results of fits to $\rho^0$ and background (see text).

4. Distribution of $d\sigma/dy_{c.m.}$ for the reaction $\gamma p \to \rho^0 X$ at $E_\gamma = 2.8$, 4.7, and 9.3 GeV.

5. Inelastic structure function F(x) for the reaction $\gamma p \to \rho^0 X$ at $E_\gamma = 2.8$ and 4.7 GeV.

6. Inelastic structure function F(x) for the reaction $\gamma p \to \rho^0 X$ at $E_\gamma = 9.3$ GeV (full circles), together with F(x) for $\rho^0$ production via SCHC and natural-parity exchange (Diffractive - open squares). The curve shows F(x) for $\gamma p \to \pi^- X$ at the same energy [7], multiplied by the ratio of $\rho^0$ to $\pi^-$ multiplicities.

7. Decay angular distribution of $\pi^+\pi^-$ pairs in the $\rho$ mass band with $x > 0.8$ at $E_\gamma = 9.3$ GeV. The helicity (H), Gottfried-Jackson (GJ), and Adair (A) reference systems are used. For definition of the angles see text.

8. The $\pi^+\pi^-$ mass distributions at $E_\gamma = 4.7$ and 9.3 GeV in the two forward x intervals (histograms), with the moment II described in the text superimposed as full points. The curves are the results of the fits to the mass distributions.

9. Inelastic structure functions F(x), normalized to the inelastic cross sections, for the reactions $\gamma p \to \rho^{o}X$ at $E_{\gamma} = 9.3$ GeV (data points), $\pi^{+}p \to \pi^{+}X$ at 7 GeV/c from ref. [10] (solid curve), and $\pi^{+}p \to \rho^{o}X$ at 16 GeV/c from ref. [2b] (dashed curve).

10. Distribution of $d\sigma/dp_{T}^{2}$ for the reaction $\gamma p \to \rho^{o}X$ at $E_{\gamma} = 2.8$, 4.7, and 9.3 GeV.

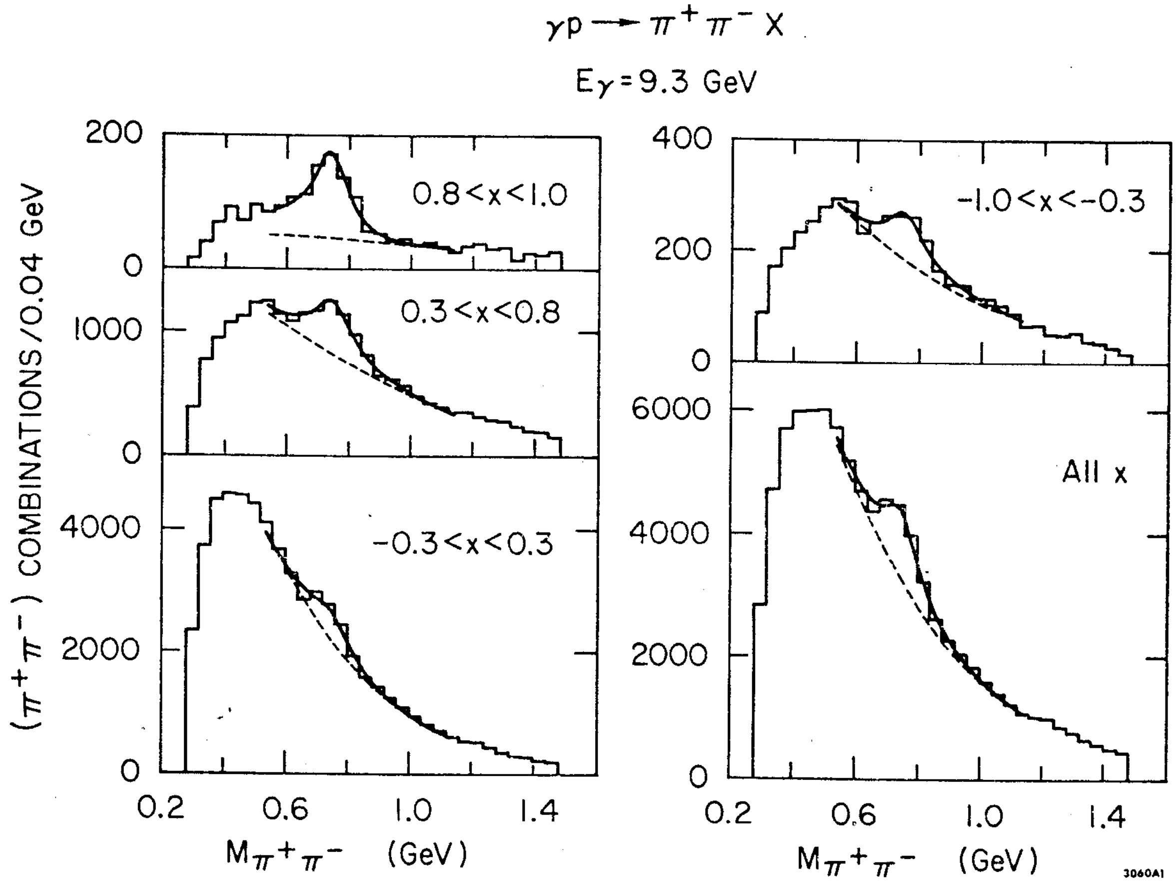

γp → π+π− X
Eγ=9.3 GeV
(π+π−) COMBINATIONS/0.04 GeV
0.8<x<1.0
0.3<x<0.8
−0.3<x<0.3
−1.0<x<−0.3
All x
Mπ+π− (GeV)
3060A1


Fig. 1

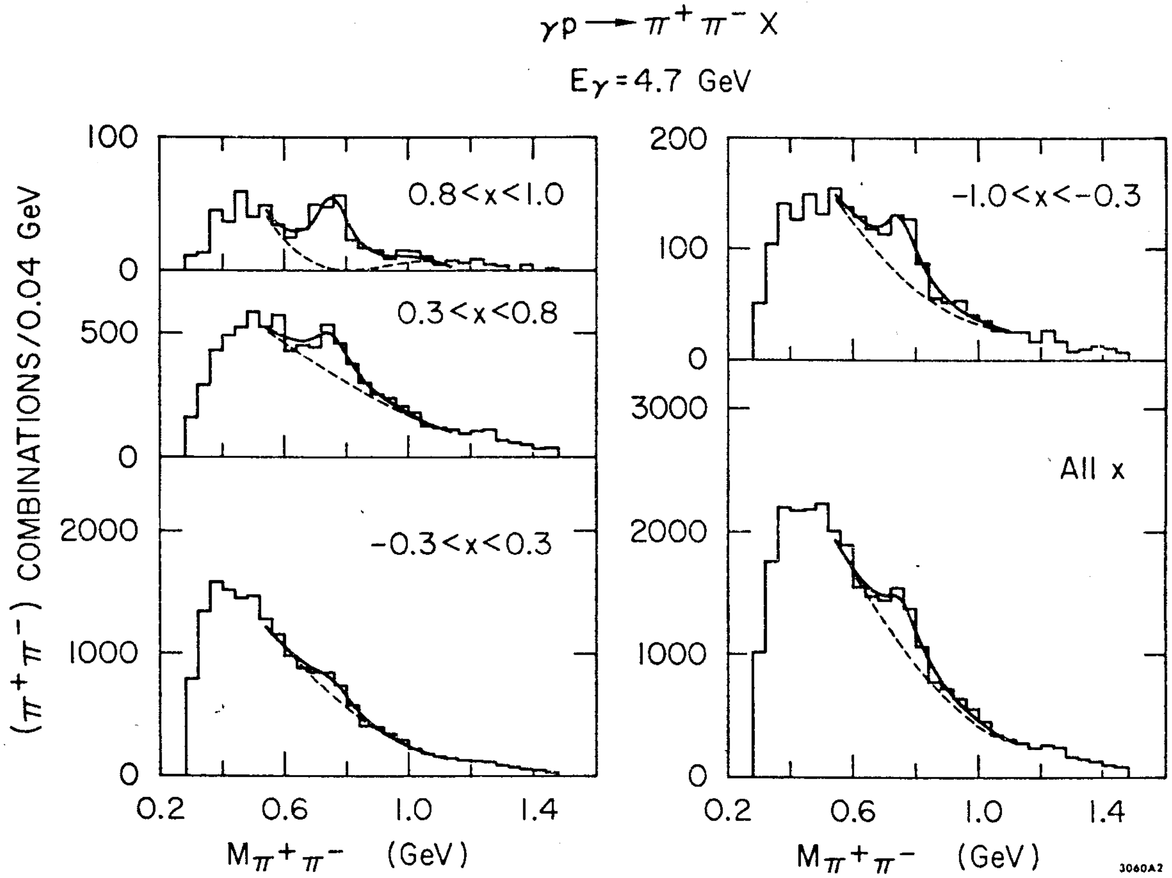

γp → π⁺π⁻ X
Eγ = 4.7 GeV
(π⁺π⁻) COMBINATIONS/0.04 GeV
0.8<x<1.0
0.3<x<0.8
-0.3<x<0.3
-1.0<x<-0.3
All x
M π⁺π⁻ (GeV)
3060A2


Fig. 2

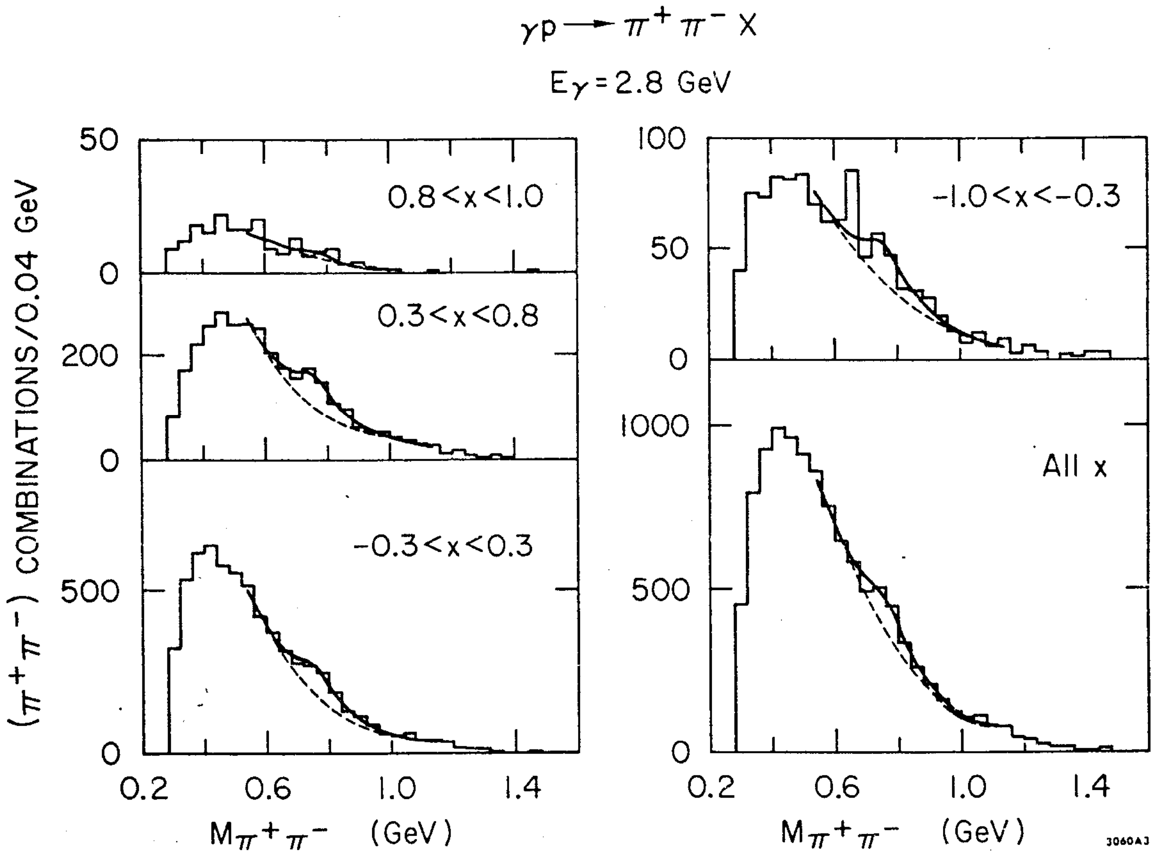

γp → π⁺π⁻ X
Eγ = 2.8 GeV
0.8<x<1.0
0.3<x<0.8
-0.3<x<0.3
-1.0<x<-0.3
All x
(π⁺π⁻) COMBINATIONS/0.04 GeV
Mπ⁺π⁻ (GeV)
3060A3


Fig. 3

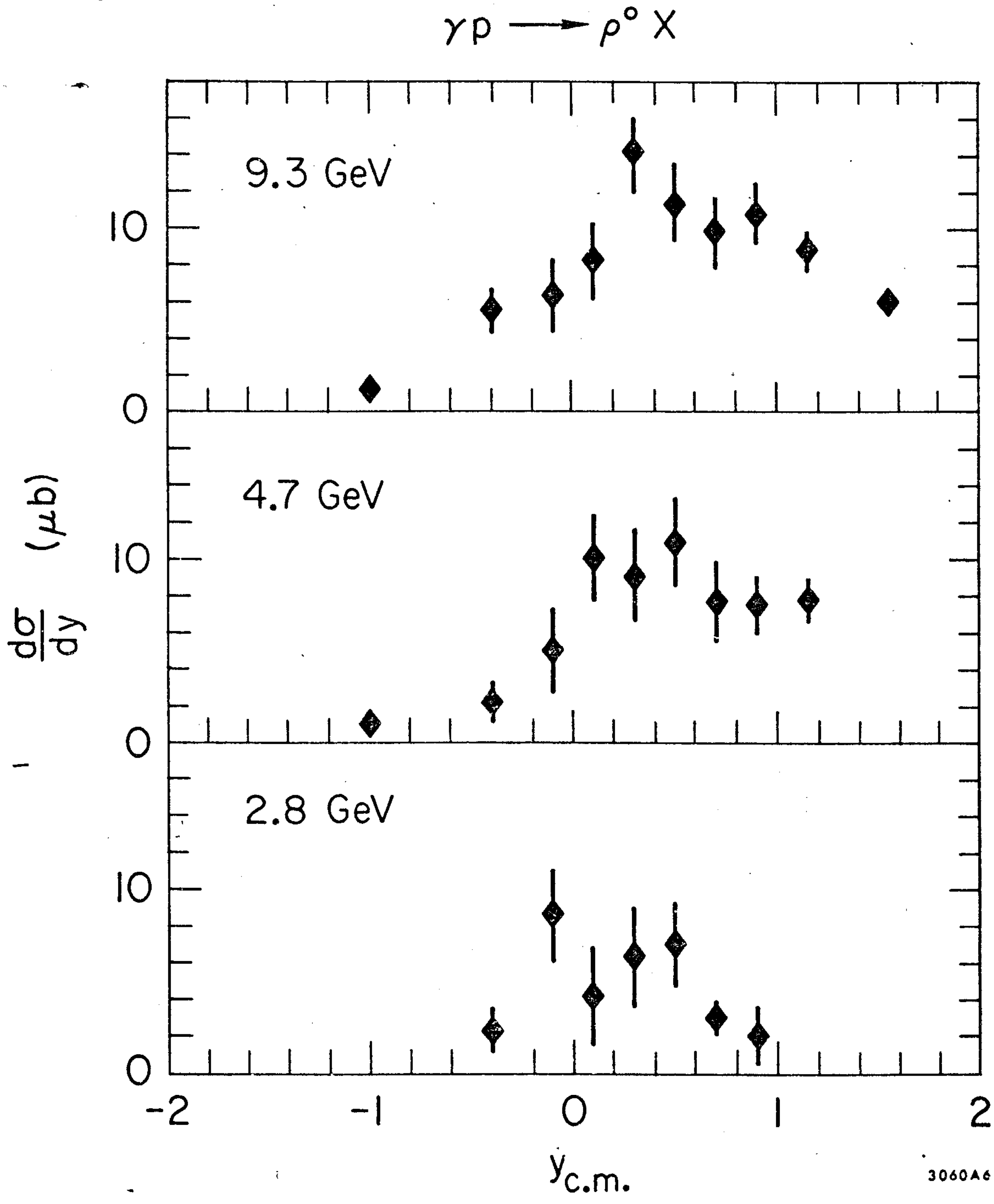


Fig. 4

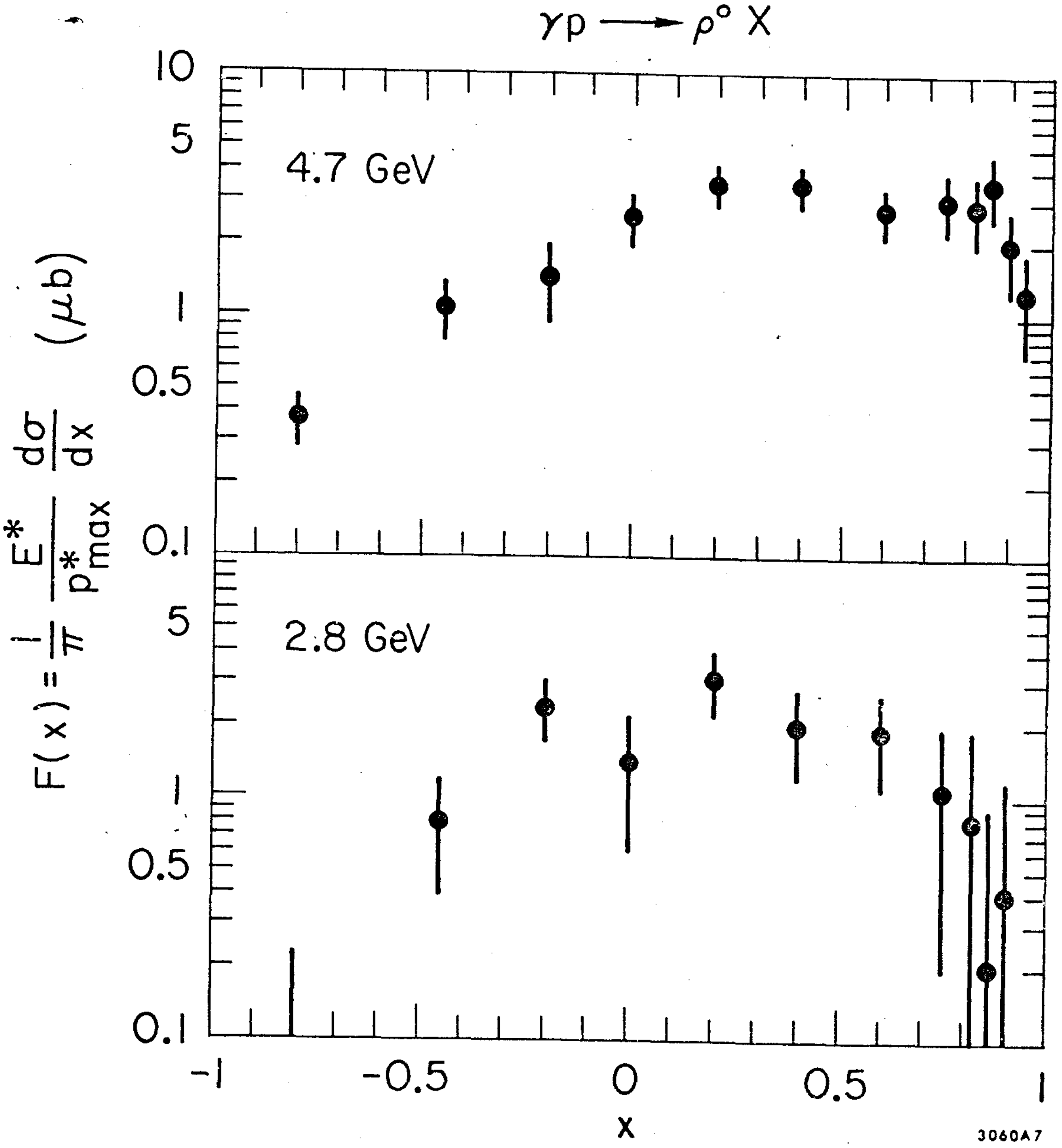

γp ⟶ ρ° X
4.7 GeV
2.8 GeV
F(x) = 1/π E*/p*max dσ/dx (μb)
10
5
1
0.5
0.1
-1
-0.5
0
0.5
1
x
3060A7


Fig. 5

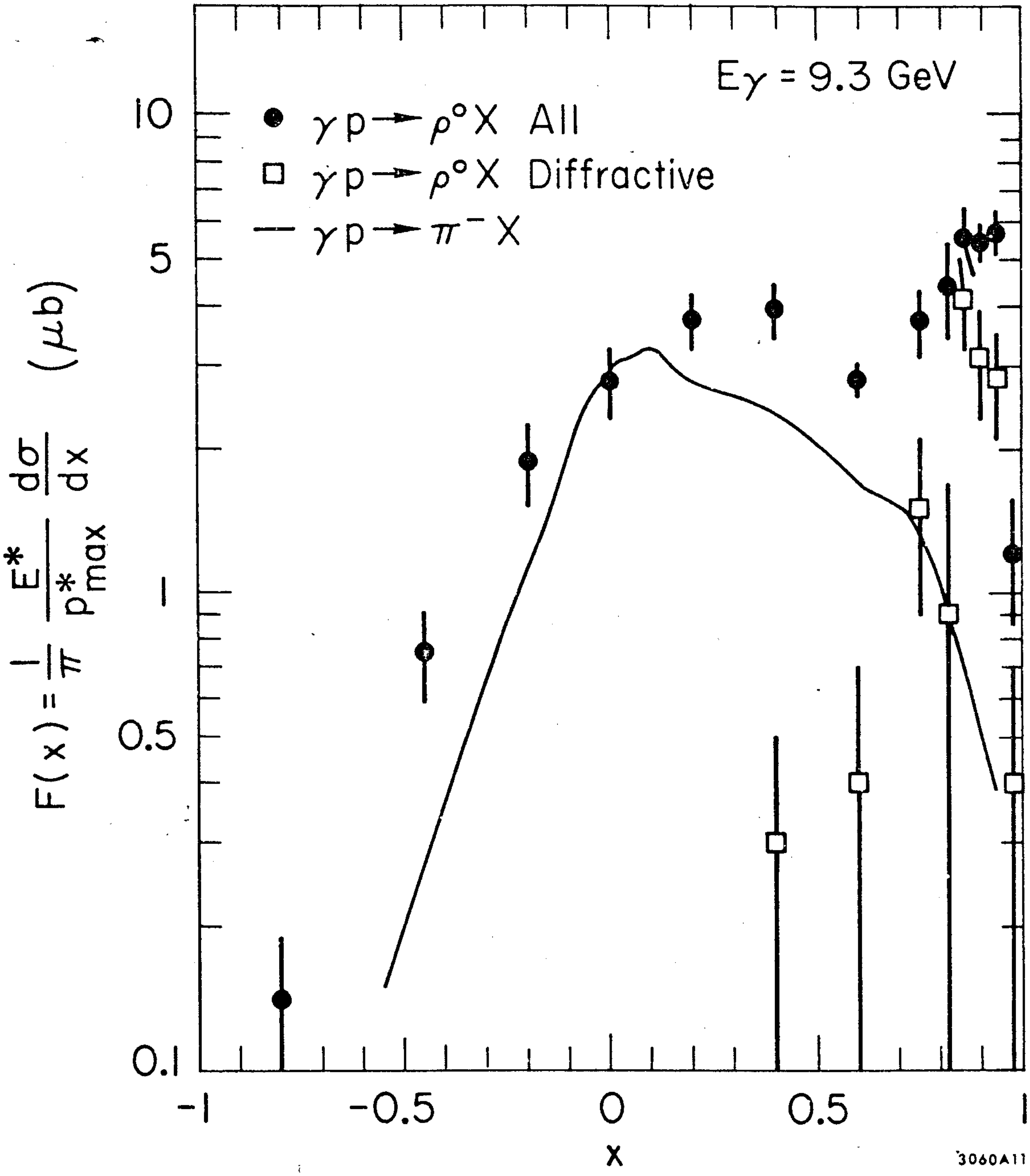

Eγ = 9.3 GeV
γp → ρ°X All
γp → ρ°X Diffractive
γp → π⁻X
F(x) = 1/π E*/p*max dσ/dx (μb)
10
5
1
0.5
0.1
-1
-0.5
0
0.5
1
x
3060A11


Fig. 6

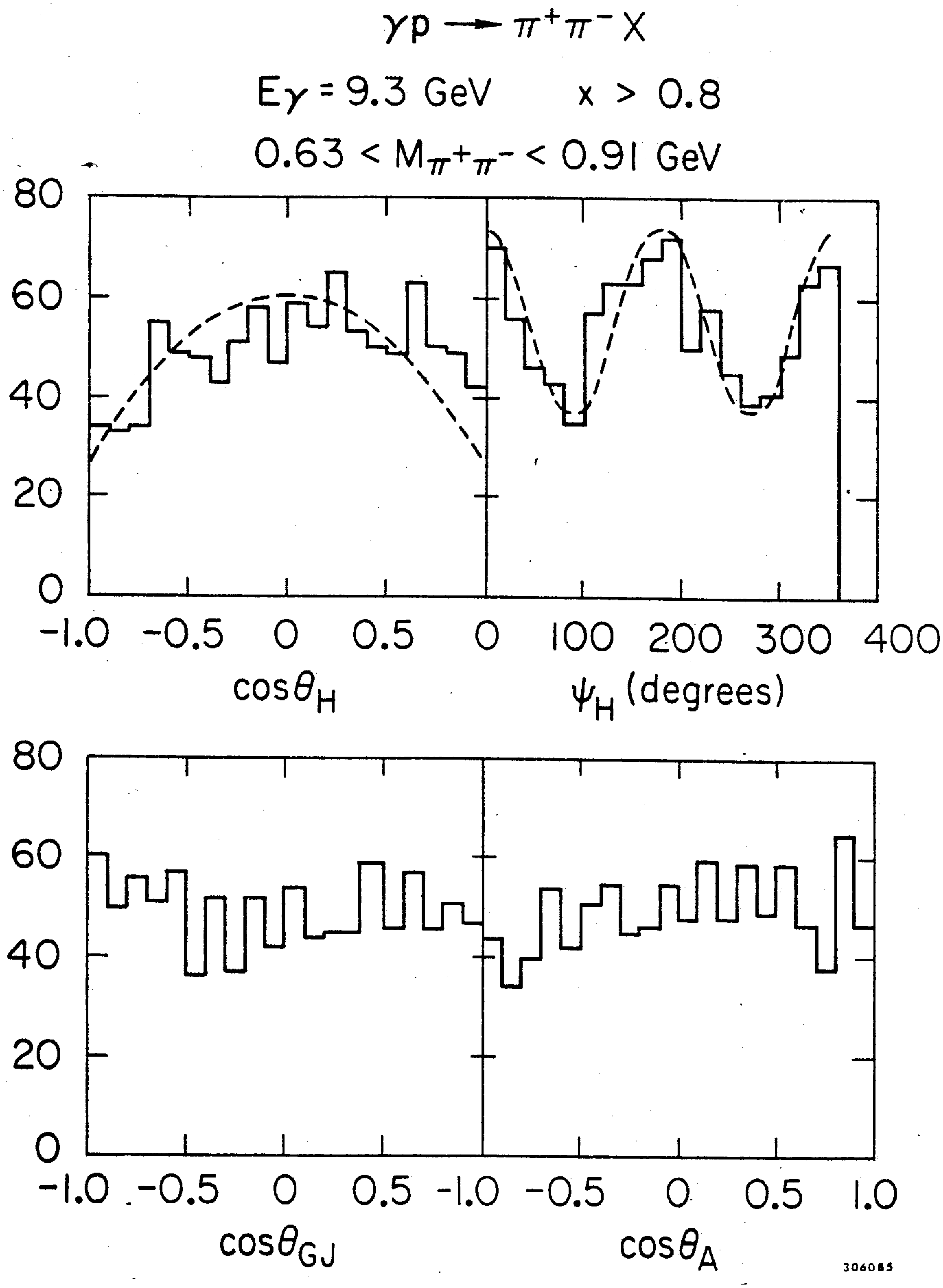

γp → π+π−X
Eγ = 9.3 GeV x > 0.8
0.63 < Mπ+π− < 0.91 GeV
80
60
40
20
0
−1.0 −0.5 0 0.5 0 100 200 300 400
cosθH
ψH (degrees)
−1.0 −0.5 0 0.5 −1.0 −0.5 0 0.5 1.0
cosθGJ
cosθA
306085


Fig. 7

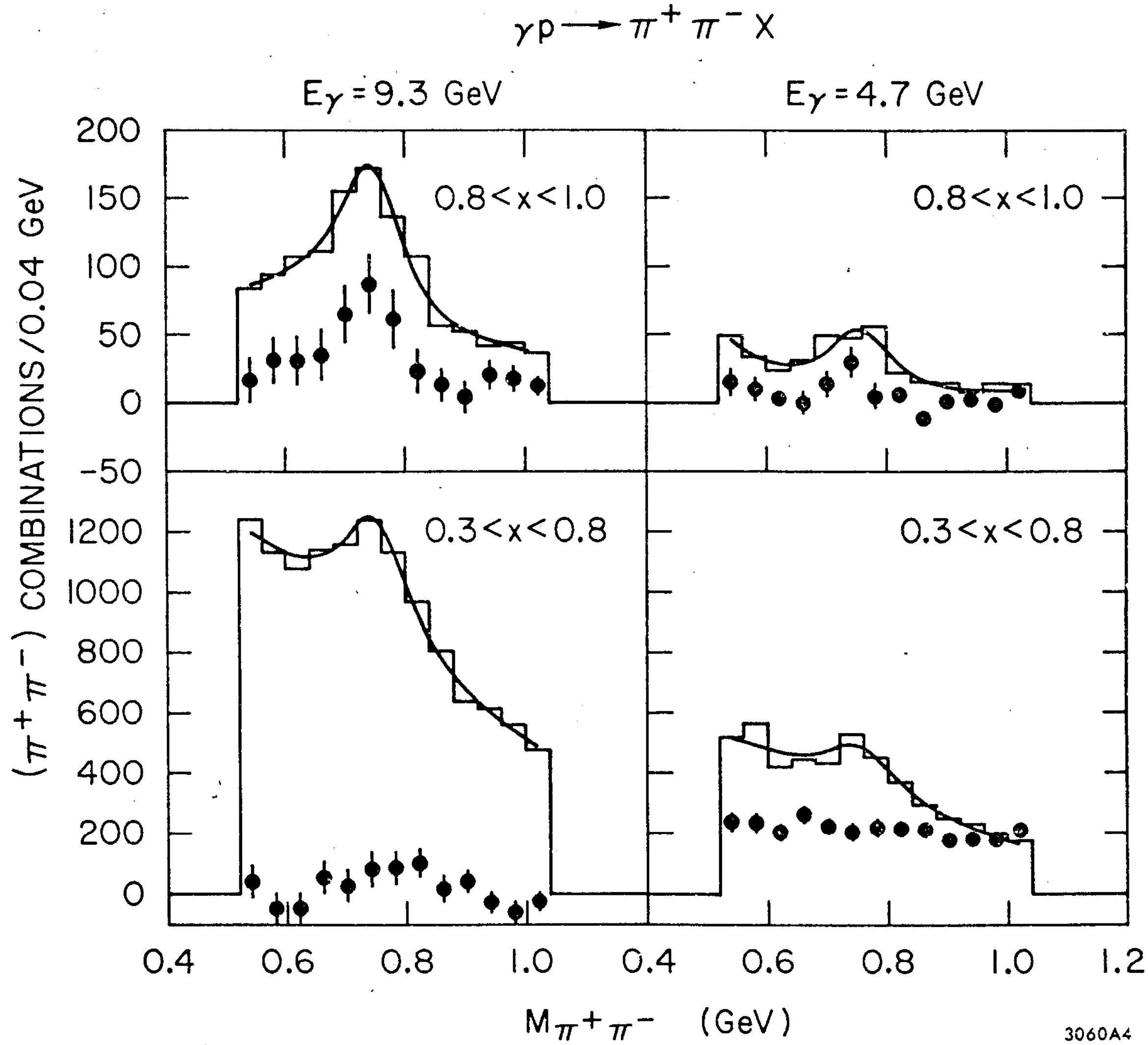

γp → π⁺ π⁻ X
Eγ = 9.3 GeV
Eγ = 4.7 GeV
0.8<x<1.0
0.8<x<1.0
0.3<x<0.8
0.3<x<0.8
(π⁺π⁻) COMBINATIONS/0.04 GeV
M π⁺π⁻ (GeV)
3060A4


Fig. 8

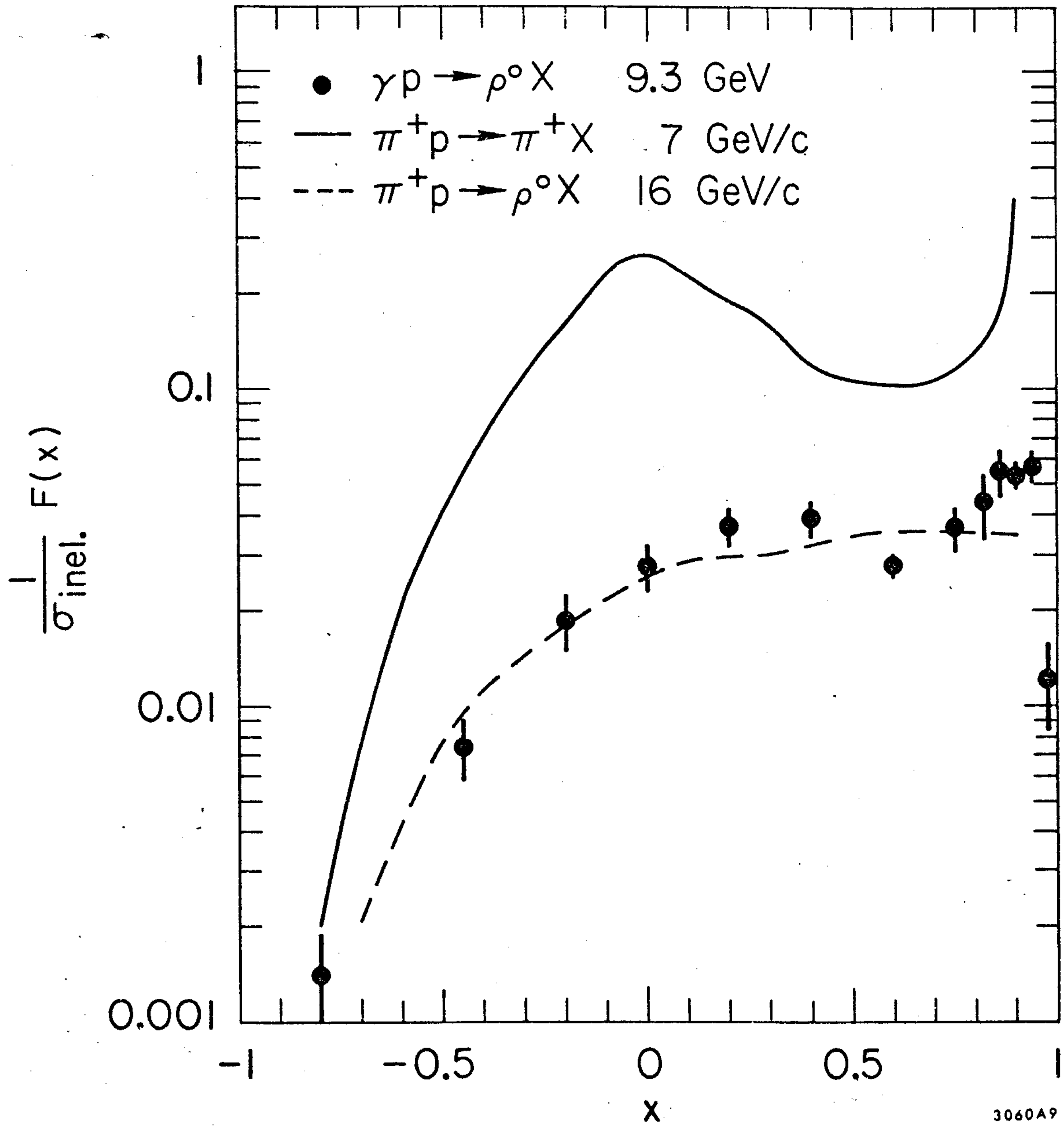

γp → ρ°X 9.3 GeV
π⁺p → π⁺X 7 GeV/c
π⁺p → ρ°X 16 GeV/c
1
0.1
0.01
0.001
1/σ_inel. F(x)
−1
−0.5
0
0.5
1
x
3060A9


Fig. 9

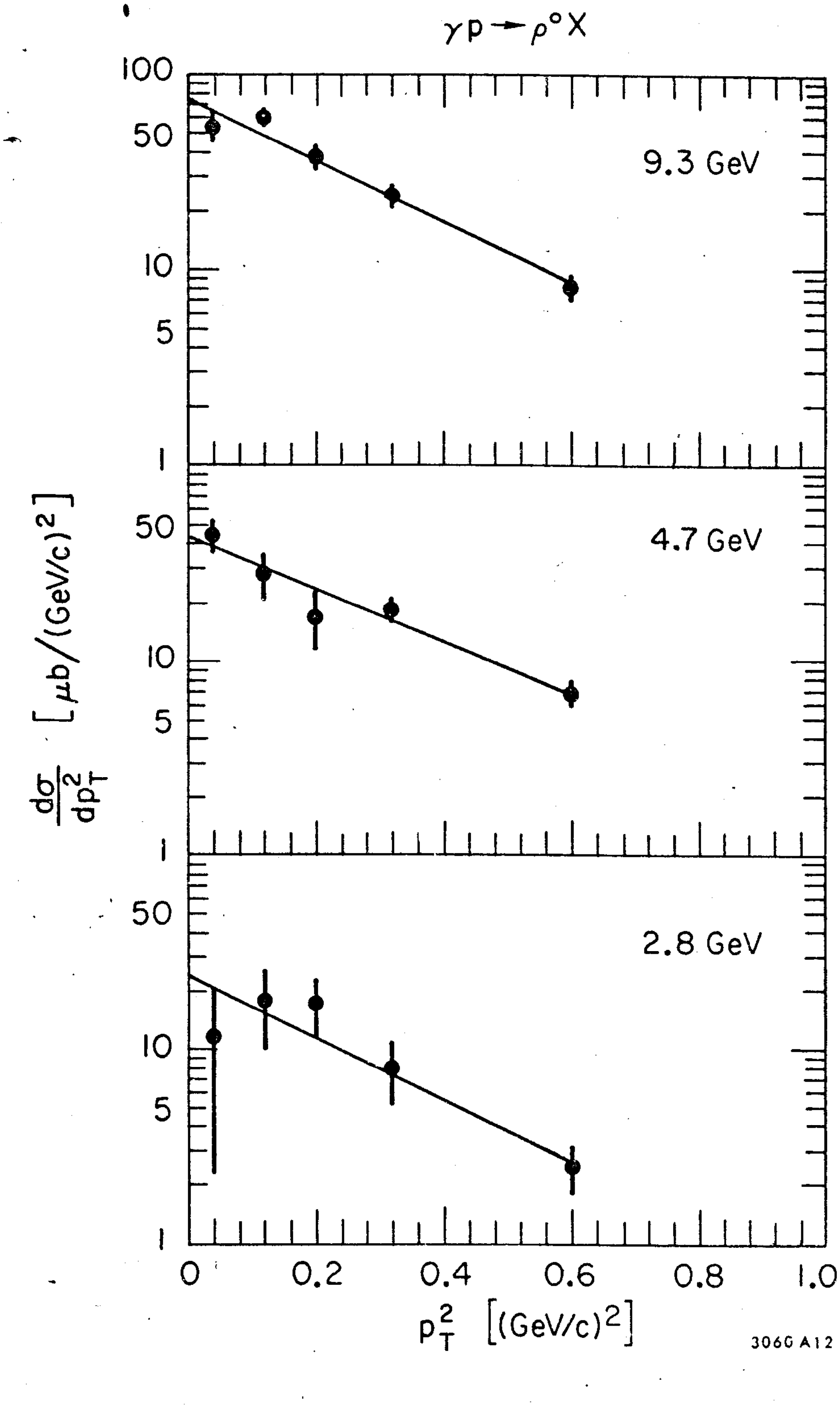

$\gamma p \to \rho^\circ X$
9.3 GeV
4.7 GeV
2.8 GeV
$\frac{d\sigma}{dp_T^2}$ $[\mu b/(GeV/c)^2]$
$p_T^2$ $[(GeV/c)^2]$
100
50
10
5
1
0
0.2
0.4
0.6
0.8
1.0
3060A12


Fig. 10